XL CILAMCE
IBERO-LATIN AMERICAN CONGRESS ON COMPUTATIONAL METHODS IN ENGINEERING
NOVEMBER 11-14, 2019
Praiamar Natal Hotel & Convention
Natal, RN-BRAZIL

NUMERICAL ASSESSMENT OF A STRESS RECOVERY PROCEDURE APPLIED TO STABLE GFEM USING FLAT-TOP PARTITION OF UNITY

Murilo H. C. Bento
Caio S. Ramos
m.bento@usp.br
caio_silva@usp.br
Department of Structural Engineering, São Carlos School of Engineering, University of São Paulo
Avenida Trabalhador São Carlense, 400, 13566-590, São Carlos, SP, Brasil
Rafael Marques Lins
mlins@ita.br
Aeronautics Technological Institute (ITA)
Praça Marechal Eduardo Gomes, 50, 12228-900, São José dos Campos, SP, Brasil
Sergio P. B. Proença
persival@sc.usp.br
Department of Structural Engineering, São Carlos School of Engineering, University of São Paulo
Avenida Trabalhador São Carlense, 400, 13566-590, São Carlos, SP, Brasil

Abstract. The Generalized Finite Element Method (GFEM) is a Galerkin method based on augmenting low-order FE approximation spaces with functions that well represent local behaviors of the solution. Since its proposition, the method has demonstrated good performance and has provided higher-order convergence rates. A particular drawback related to it, however, is the possibility of linear dependencies between its shape functions, which leads to loss of accuracy and convergence rates decrease. In this context, stable versions for the method, with modifications in the enrichment functions and Partitions of Unity (PU), were developed aiming to eliminate these dependencies and keep GFEM optimal convergence rates. On the other hand, it is known that for displacement formulations the stress field coming from numerical approaches is less accurate than the main displacement field. Very recently, a stress recovery procedure was proposed for Stable GFEM (SGFEM). This process is based on a weighted L^2 inner product, which leads to a block-diagonal matrix, being therefore very efficient. In this work, we aim to assess this recovery procedure when applied to SGFEM using Flat-Top PU for quadrilateral FE meshes. In particular, we evaluate the effect of using Lagrangian PU for weighting the L^2 inner product used to generate the recovered stress field and the conditioning of this system coefficient matrix. Numerical examples show that the combination of this GFEM version and the recovery procedure in addition to guaranteeing stability for the solution also provides very accurate stress distributions.

Keywords: SGFEM, Flat-Top PU, Recovery Procedure, Conditioning.

1 Introduction

The use of numerical methods to solve complex engineering problems has become quite common since exact solutions are very limited. One of these methods that is currently applied as an efficient alternative to obtain solutions with good accuracy is the Generalized Finite Element Method (GFEM) (Duarte et al. [1], Strouboulis et al. [2]). The GFEM is a Galerkin method that proposes the generation of numerical approximations belonging to a space obtained by augmenting low-order standard finite element approximation spaces by enrichment functions that can well represent local behaviors of the solution.

Problems presenting special features such as discontinuities or high gradients can be efficiently solved by the GFEM. In particular, it is possible to insert into its approximation space functions that represent these discontinuities and high displacement gradients. This can deliver higher convergence rates and makes the mesh independent of the crack, which greatly facilitates the initial mesh generation and the possibility of crack propagation analyses (Belytschko and Black [3], Duarte et al. [4]).

Despite its efficacy, a particular drawback related to the GFEM, in general, is the possibility of linear dependencies between its shape functions. In this context, stable versions for the method are being developed aiming to eliminate these dependencies and keep GFEM optimal convergence rates. A recent stable version (Zhang et al. [5]) indicates the use of modified enrichment functions as proposed by Babuška and Banerjee [6] along with special Partitions of Unity (PU) for construction of the enriched space. These modifications in both the enrichment functions and the PU tries to eliminate dependencies between the conventional finite element space and the enriched one, besides some dependencies that can appear in the basis functions used in the enriched space generation.

Conventionally, displacement formulations of the Principle of Virtual Work (PVW) are used to construct the weak form of the variational problem to be studied. For problems of Continuum Mechanics, all expressions related to stress and strain fields are written in function of the displacement field using the stress-strain (constitutive equations) and strain-displacement (compatibility) relations. The only variable to be approximated in the problem is thus the displacement field. Consequently, the stress and strain fields computed by a numerical approach (GFEM or its related versions) end up being less accurate than the displacement field, once those fields are related to its derivative. One possibility to overcome this issue is to use a stress recovery procedure. This idea was explored by Lins et al. [7] very recently for the Stable GFEM (SGFEM) (Babuška and Banerjee [6] and Gupta et al. [8]). Fundamentally, this recovery procedure is based on a weighted L^2 inner product, which leads to a system of equations formed by a block-diagonal matrix, being therefore very efficient and expending few computational resources.

In this work, we aim to assess the recovery procedure exposed in the last paragraph when applied to SGFEM with Flat-Top PU (SGFEM$^{\text{FT}}$) for the construction of the enrichment function space for 2D quadrilateral finite element meshes (Sato et al. [9]). In particular, we evaluate the effect of adopting Lagrangian PU for weighting the L^2 inner product used to construct the system of equations that generates the recovered stress field. Following this introduction, the problem type formulation and the numerical methods used herein are addressed in Section 2. Section 3 presents the stress recovery procedure proposed by Lins et al. [7]. Section 4 shows some numerical examples related to the application of the stress recovery procedure and, finally, Section 5 exhibits the main conclusions of this work.

2 Numerical Approaches

2.1 Problem formulation

Consider a two-dimensional domain $\Omega \subset \mathbb{R}^2$ with boundary $\partial\Omega$ that can be decomposed in the regions $\partial\Omega^u$ and $\partial\Omega^\sigma$ where Dirichlet and Neumann boundary conditions are applied, respectively. $\partial\Omega^u$ and $\partial\Omega^\sigma$ consists of a partition of $\partial\Omega$, i.e., $\partial\Omega^u \cup \partial\Omega^\sigma = \partial\Omega$ and $\partial\Omega^u \cap \partial\Omega^\sigma = \varnothing$. In addition, consider a traction-free domain crack Γ_C where the displacement field is discontinuous.

The problem consists of finding a displacement field $\mathbf{u}$, such that it satisfies the governing equations, which can be separated in equilibrium, constitutive and compatibility equations:

$$\operatorname{div}(\boldsymbol{\sigma}) + \bar{\mathbf{b}} = \mathbf{0} \tag{1}$$

$$\boldsymbol{\sigma} = \mathbb{C} : \boldsymbol{\varepsilon}, \tag{2}$$

$$\boldsymbol{\varepsilon} = \nabla_s \mathbf{u} = \frac{1}{2}\left((\nabla \mathbf{u})^{\mathrm{T}} + \nabla \mathbf{u}\right). \tag{3}$$

In equations 1–3, $\boldsymbol{\sigma}$ and $\boldsymbol{\varepsilon}$ represents the Cauchy stress and the infinitesimal strain tensors, respectively. $\mathbb{C}$ represents the fourth-order elastic constitutive tensor and $\bar{\mathbf{b}}$ the domain forces vector.

Besides the relations 1–3, the solution fields have to satisfy all boundary conditions applied to the solid, i.e., $\mathbf{u} = \bar{\mathbf{u}}$ on $\partial\Omega^u$, and $\boldsymbol{\sigma} \,.\, \mathbf{n} = \bar{\mathbf{t}}$ on $\partial\Omega^\sigma$. In these relations, $\bar{\mathbf{u}}$ and $\bar{\mathbf{t}}$ are prescribed displacements and tractions and $\mathbf{n}$ is an outward unit vector normal to $\partial\Omega^\sigma$. Finally, along the crack line the traction vector vanishes, i.e., $\boldsymbol{\sigma} \,.\, \mathbf{n} = \mathbf{0}$ on Γ_C.

In a weak sense, the same problem can be formulated using the PVW, which states:

Find $\mathbf{u} \in \mathbf{X}(\Omega) \subset (H^1(\Omega))^2$, that $\forall \delta\mathbf{u} \in \mathbf{Y}(\Omega) \subset (H^1(\Omega))^2$,

$$\int_\Omega \boldsymbol{\sigma}(\mathbf{u}) : \boldsymbol{\varepsilon}(\delta\mathbf{u})\, \mathrm{d}\Omega = \int_\Omega \bar{\mathbf{b}} \cdot \delta\mathbf{u}\, \mathrm{d}\Omega + \int_{\partial\Omega^\sigma} \bar{\mathbf{t}} \cdot \delta\mathbf{u}\, \mathrm{d}\Gamma. \tag{4}$$

In Eq. 4, $\mathbf{X}(\Omega)$ and $\mathbf{Y}(\Omega)$ are respectively the spaces used for the definition of trial functions, in which $\mathbf{u}(\mathbf{x}) = \bar{\mathbf{u}}$ for $\mathbf{x} \in \partial\Omega^u$, and test functions, in which $\delta\mathbf{u}(\mathbf{x}) = \mathbf{0}$ for $\mathbf{x} \in \partial\Omega^u$. In addition, $H^1(\Omega)$ is the Sobolev space of functions on Ω with generalized derivatives $L^2(\Omega)$.

2.2 GFEM

The Generalized Finite Element Method (GFEM) is a Galerkin method that generates numerical solutions belonging to a space obtained by augmenting low-order finite element approximation spaces with functions that well represent local behaviors of the problem solution. In its context, these functions are known as enrichment functions and they are usually introduced by previous knowledge about the problem exact (or, at least, expected) solution.

Accordingly, the GFEM approximation space can be written as the sum between the conventional FEM approximation space $\mathcal{S}_{\text{FEM}}$ and the space $\mathcal{S}_{\text{ENR}}$ spanned by the adopted enrichment functions, i.e.,

$$\mathcal{S}_{\text{GFEM}} \coloneqq \mathcal{S}_{\text{FEM}} + \mathcal{S}_{\text{ENR}}. \tag{5}$$

For being an instance of the Partition of Unity Methods (PUM) (Melenk and Babuška [10]), the GFEM shape functions are build as the product between nodal linear or bi-linear Lagrangian PU (which also defines FEM shape functions) and a set of enrichment functions defined on each node:

$$\phi_{\alpha i} = \varphi_\alpha L_{\alpha i} \quad (\text{no summation on } \alpha). \tag{6}$$

In Eq. 6, φ_α refers to a PU component related to discretization cloud α, and $L_{\alpha i},\ i \in \mathscr{I}_\alpha$ refers to the i^{th} enrichment function belonging to the vector $\mathbf{L}_\alpha$, with $\mathscr{I}_\alpha$ being an index set associated to the adopted enrichment functions.

A global approximation $\hat{\mathbf{u}}$ for displacement vector field can now be defined using that shape functions (Eq. 6). Equation 7 presents this approximation where $\mathbf{u}_{\alpha i}$ refers to the coefficients (generalized

degrees of freedom) used for constructing $\hat{\mathbf{u}}$ as a linear combination of $\phi_{\alpha i}$.

$$\hat{\mathbf{u}} = \sum_{\alpha=1}^{N} \sum_{i \in \mathscr{I}_\alpha} \mathbf{u}_{\alpha i} \phi_{\alpha i} = \sum_{\alpha=1}^{N} \varphi_\alpha \sum_{i \in \mathscr{I}_\alpha} \mathbf{u}_{\alpha i} L_{\alpha i} = \sum_{\alpha=1}^{N} \varphi_\alpha \hat{\mathbf{u}}_\alpha. \tag{7}$$

Noticeably, the global approximation can be understood in Eq. 7 as gluing local approximation functions $\hat{\mathbf{u}}_\alpha \in \chi_\alpha(\omega_\alpha) = \text{span}(L_{\alpha i})_{i \in \mathscr{I}_\alpha}$ using a PU to construct globally conforming approximate solutions.

In the GFEM context, it is usually considered $L_{\alpha 1} = 1$, $\forall \alpha$, and thus GFEM can restore FEM solutions. Hence, Eq. 7 can be conveniently split into two parts, as:

$$\hat{\mathbf{u}} = \sum_{\alpha=1}^{N} \mathbf{u}_{\alpha 1} \varphi_\alpha + \sum_{\alpha=1}^{N} \varphi_\alpha \sum_{i \in \mathscr{I}_\alpha,\, i \neq 1} \mathbf{u}_{\alpha i} L_{\alpha i} = \hat{\mathbf{u}}_{\text{FEM}} + \hat{\mathbf{u}}_{\text{ENR}}. \tag{8}$$

Based on Eq. 8, the GFEM approximation spaces can be expressed by:

$$\mathcal{S}_{\text{FEM}} = \left\{ \zeta \colon \zeta = \sum_{\alpha=1}^{N} c_\alpha \varphi_\alpha,\ c_\alpha \in \mathbb{R} \right\} \tag{9}$$

$$\mathcal{S}_{\text{ENR}} = \left\{ \zeta \colon \zeta = \sum_{\alpha=1}^{N} \varphi_\alpha \chi_\alpha^{\text{ENR}},\ \chi_\alpha^{\text{ENR}} = \text{span}(L_{\alpha i})_{i \in \mathscr{I}_\alpha,\, i \neq 1} \right\}. \tag{10}$$

2.3 A GFEM stable version

Firstly, we define the measure used herein to evaluate the stiffness matrix conditioning. Let $\mathfrak{R}(\mathbf{K})$ be the Scaled Condition Number (SCN) of a stiffness matrix $\mathbf{K}$ given by GFEM or its stable versions. Because $\mathbf{K}$ is a symmetric positive-definite matrix, Babuška and Banerjee [6] define $\mathfrak{R}(\mathbf{K}) \coloneqq \kappa_2(\mathbf{H})$, where $\kappa_2(\mathbf{H}) = \|\mathbf{H}\|_2 \|\mathbf{H}^{-1}\|_2$ is the condition number of $\mathbf{H}$ based on the L^2 matrix norm and $\mathbf{H} = \mathbf{DKD}$, where $\mathbf{D}$ is a diagonal matrix with diagonal entries $D_{ii} = 1/\text{sqrt}(K_{ii})$. It must be highlighted that the SCN also can be defined as $\kappa_2(\mathbf{H}) = \lambda_M/\lambda_m$, in which λ_M and λ_m are the largest and smallest eigenvalues of $\mathbf{H}$, respectively.

Babuška and Banerjee [6] and Gupta et al. [8] have already presented that even for smooth enrichment functions $L_{\alpha i} \in \chi_\alpha(\omega_\alpha)$ the stiffness matrix SCN rate is orders of $\mathfrak{R}(\mathbf{K}_{\text{GFEM}}) = \mathcal{O}(h^{-4})$, with h being a finite element size for uniform meshes. This rate is orders of magnitude greater than $\mathfrak{R}(\mathbf{K}_{\text{FEM}}) = \mathcal{O}(h^{-2})$.

Trying to reduce the SCN when GFEM is used, Babuška and Banerjee [6] propose a simple modification to be applied in the enrichment functions that generates the enriched approximation space $\tilde{\mathcal{S}}_{\text{ENR}}$. The modified enrichment functions $\tilde{L}_{\alpha i}$ are given by

$$\tilde{L}_{\alpha i}(\mathbf{x}) = L_{\alpha i}(\mathbf{x}) - \mathcal{I}_{\omega_\alpha}[L_{\alpha i}](\mathbf{x}) \tag{11}$$

where $\mathcal{I}_{\omega_\alpha}[L_{\alpha i}]$ is the piecewise linear or bi-linear finite element interpolant of $L_{\alpha i}$, which for an arbitrary integration point (ξ, η) is given by

$$\mathcal{I}_{\omega_\alpha}[L_{\alpha i}](\xi, \eta) = \sum_{j=1}^{n} \varphi_j(\xi, \eta)\, L_{\alpha i}(\mathbf{x}_j) \tag{12}$$

with n equals to the finite element number of nodes.

Even with the modifications proposed by Babuška and Banerjee [6], the stiffness matrix conditioning could not be controlled in 2D and 3D analysis when some combinations of enrichment functions were applied (Zhang et al. [5]). Later, Zhang et al. [5] have then proposed another modification to be imposed in the enriched approximation space generation.

This modification consists of using another PU φ^* to generate $\tilde{\mathcal{S}}_{\text{ENR}}$. In this case, the approximation $\hat{\mathbf{u}}$ can be written as:

$$\hat{\mathbf{u}} = \sum_{\alpha=1}^{N} \mathbf{u}_{\alpha 1}\varphi_\alpha + \sum_{\alpha=1}^{N} \varphi_\alpha^* \sum_{i\in\mathscr{I}_\alpha,\, i\neq 1} \mathbf{u}_{\alpha i}\left(L_{\alpha i} - \mathcal{I}_{\omega_\alpha}[L_{\alpha i}]\right) \tag{13}$$

In this paper, we adopt to φ^* a Flat-Top PU as proposed by Zhang et al. [5] and used by Sato et al. [9] in 2D analysis with quadrilateral finite elements.

For a 1D master element, the Flat-Top PU components are illustrated in Fig. 1 and the reader is referred to Zhang et al. [5] and Sato et al. [9] for their expressions. In this paper, we adopt the values suggested by Sato et al. [9] for the parameters that define the Flat-Top PU, i.e., $\sigma = 0.1$ and $l = 1$.

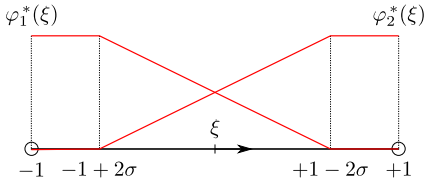

Figure 1. 1D Flat-Top PU components on a master element

$\tau_{\text{L}} = \{\xi \in \mathbb{R} / -1 \leq \xi \leq 1\}$.

For a 2D master quadrilateral element $\tau_{\text{Q}} = \left\{(\xi,\eta) \in \mathbb{R}^2 / -1 \leq \xi \leq 1 \text{ and } -1 \leq \eta \leq 1\right\}$, the Flat-Top PU components are obtained by a tensorial product between φ_1^* and φ_2^*, resulting:

$$\varphi_1^{\tau_{\text{Q}}\,*}(\xi,\eta) = \varphi_1^*(\xi)\,\varphi_1^*(\eta) \tag{14}$$
$$\varphi_2^{\tau_{\text{Q}}\,*}(\xi,\eta) = \varphi_2^*(\xi)\,\varphi_1^*(\eta) \tag{15}$$
$$\varphi_3^{\tau_{\text{Q}}\,*}(\xi,\eta) = \varphi_1^*(\xi)\,\varphi_2^*(\eta) \tag{16}$$
$$\varphi_4^{\tau_{\text{Q}}\,*}(\xi,\eta) = \varphi_2^*(\xi)\,\varphi_2^*(\eta) \tag{17}$$

Figure 2 presents a illustration of 2D Flat-Top PU for quadrilateral elements. The method in which the approximation $\hat{\mathbf{u}}$ is constructed based on Eq. 13 with Flat-Top PU is herein denoted as SGFEM$^{\text{FT}}$.

3 A Stress Recovery Procedure

In this section, the stress recovery procedure to be evaluated in this paper is addressed. This recovery procedure, recently proposed by Lins et al. [7], introduces a generalization of the recovery procedures developed by Prange et al. [11] for the eXtended Finite Element Methof (XFEM) (Belytschko and Black [3], Moes et al. [12]) and also by Lins et al. [13] for the SGFEM.

For stress recovery procedures, the components of the recovered stress field $\boldsymbol{\sigma}^*$ are written as a linear combination of the shape functions used to define the approximate displacement field, i.e.,

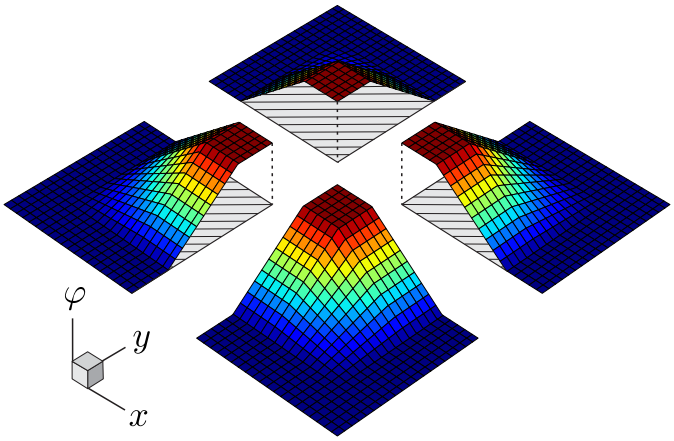

Figure 2. 2D Flat-Top PU components on quadrilateral finite elements.
Adapted from Ramos [14].

$$\boldsymbol{\sigma}^* = \sum_{\alpha=1}^{N} \varphi_\alpha \mathbf{a}_{\alpha 1} + \sum_{\alpha=1}^{N} \varphi_\alpha \sum_{i \in \mathscr{I}_\alpha,\, i \neq 1} \mathbf{a}_{\alpha i}\, L^*_{\alpha i}. \tag{18}$$

In Eq. 18, the same enrichment functions that generate $\hat{\mathbf{u}}$ are used to construct the recovered stress field, i.e., $L^*_{\alpha i} = L_{\alpha i}$, except for the cases of branch functions as those adopted in Example 4.2. The functions used for these cases can be found in Lins et al. [7].

The new methodology proposed by Lins et al. [7] is based on a local weighted L^2 projection as the one presented by Schweitzer [15] for construction of lumped mass matrices for dynamic problems using Partition of Unity Methods (PUM). Basically, a system of equations is solved for obtaining all components of the recovered stress field and this system can be written as

$$\tilde{A}^{\,d}_{(\alpha,i),(\beta,j)} \cdot \tilde{a}^{\,d}_{(\alpha,i)} = f^{\,d}_{(\beta,j)}, \tag{19}$$

in which α and β refer to discretization clouds, i and j to each component of the enrichment functions vectors $\mathbf{L}_\alpha$ and $\mathbf{L}_\beta$, respectively, and $d = 1, 2, 3$ refers to each stress field component (for the 2D case).

The methodology proposed by the authors understands the entries of the independent vector of Eq. 19, $f^{\,d}_{(\beta,j)}$, as the L^2 inner product between $\hat{\sigma}^d$ and $L^d_{\beta j}$ weighted by the PU component φ_β, i.e.,

$$f^{\,d}_{(\beta,j)} = \int_\Omega \hat{\sigma}^d \varphi_\beta L^d_{\beta j}\, \mathrm{d}\Omega = \int_{\omega_\beta} \hat{\sigma}^d \varphi_\beta L^d_{\beta j}\, \mathrm{d}\Omega := \left(\hat{\sigma}^d, L^d_{\beta j}\right)^{\varphi_\beta}_{L^2(\omega_\beta)} \tag{20}$$

where $\hat{\sigma}^d$ represents the components of the raw stress field given by GFEM (and its stable versions) and $L^d_{\beta j}$ represents a generic enrichment function defined over ω_β.

The same strategy can be used to calculate the entries of $\tilde{\mathbf{A}}^d$, i.e.,

$$\tilde{A}^{\,d}_{(\alpha,i),(\beta,j)} = \begin{cases} 0 & \text{if} \quad \alpha \neq \beta \\ \left(L^d_{\alpha i}, L^d_{\beta j}\right)^{\varphi_\beta}_{L^2(\omega_\beta)} & \text{if} \quad \alpha = \beta \end{cases} \tag{21}$$

with

$$\left(L^d_{\alpha i}, L^d_{\beta j}\right)^{\varphi_\beta}_{L^2(\omega_\beta)} = \int_{\omega_\beta} \left(L^d_{\alpha i} L^d_{\beta j}\right) \varphi_\beta\, \mathrm{d}\Omega \tag{22}$$

This methodology generates a symmetric positive-definite and block-diagonal matrix $\tilde{\mathbf{A}}^d$. Each of its blocks relates to one node of the adopted discretization and the dimension of this block depends on $\dim(\mathbf{L}_\gamma)$, i.e., the number of enrichment functions defined over the cloud node (including $L_{\gamma 1} = 1$). This matrix can be written as follows:

$$\tilde{\mathbf{A}}^d = \tilde{\mathbf{B}}_1^d \oplus \cdots \oplus \tilde{\mathbf{B}}_N^d = \begin{bmatrix} \tilde{\mathbf{B}}_1^d & \cdots & \mathbf{0} \\ & \ddots & \\ \vdots & \tilde{\mathbf{B}}_\gamma^d & \vdots \\ & & \ddots \\ \mathbf{0} & \cdots & \tilde{\mathbf{B}}_N^d \end{bmatrix} \tag{23}$$

where $\tilde{\mathbf{B}}_\gamma^d = [(L_{\gamma i}^d, L_{\gamma j}^d)_{L^2(\omega_\gamma)}^{\varphi_\gamma}]$, with $i, j \in \mathscr{I}_\gamma$.

The recovery procedure herein presented is denoted by the original authors as ZZ-BD (Zienkiewicz and Zhu block-diagonal) for being based on the original Zinkiewicz and Zhu [16] recovery process. The reader is referred to Lins et al. [7] for details and results about the stress recovery procedure and the a-posteriori error estimator based on it with conventional SGFEM.

It is important to mention that Prange et al. [11] and Lins et al. [13] did not apply the modifications in the enrichment functions for construction of the recovered stress fields. In this paper, we follow this methodology and also did not apply modifications in both the enrichment functions and the PU. As a result, the matrix $\tilde{\mathbf{A}}^d$ is equal for GFEM, SGFEM and SGFEM$^{\text{FT}}$.

4 Numerical Examples

4.1 Cylinder under internal pressure

The first example presented in this paper consists of a cylinder under internal pressure $p_i = 1.0$. Its geometry and boundary conditions are illustrated in Fig. 3. It was assumed Young's modulus $E = 21000.0$, Poisson's ratio $\nu = 0.30$ and plane stress conditions. The essential (Dirichlet) boundary conditions were applied using a penalization technique, with a penalization parameter $\eta = 10^{10}$.

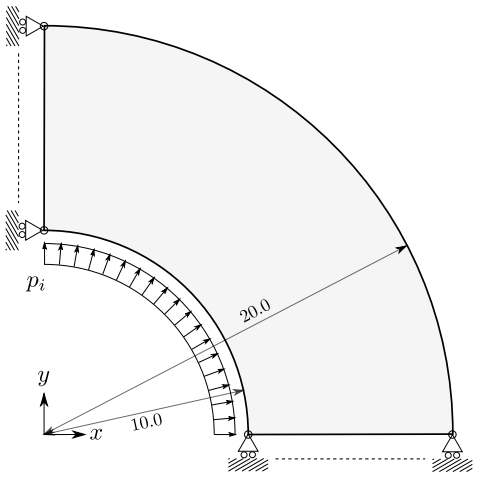

Figure 3. Cylinder under internal pressure $p_i = 1.0$.

For all analyses presented in this section, it was adopted polynomial enrichment functions of type

$$L_{\alpha i} = \frac{(x - x_\alpha)^m \, (y - y_\alpha)^n}{(\lambda_\alpha)^{m+n}}. \tag{24}$$

In Eq. 24, (x_α, y_α) are the coordinates of node α and λ_α is a cloud property known as its radius, i.e., $\lambda_\alpha = \max_j \, \mathrm{dist}(\mathbf{x}_\alpha, \mathbf{x}_j)$, with $j \in \mathrm{nodes}(\omega_\alpha)$.

For this example, it was assumed second-order complete polynomial functions $L_{\alpha i} \in \mathscr{P}^2_{\omega_\alpha}$, $\forall \alpha$ (including those in which essential boundary conditions were applied), in which $(m, n) = (1, 0) + (0, 1) + (2, 0) + (1, 1) + (0, 2)$. It is important to highlight that, for the functions generated by Eq. 24 that presents the monomials x, y and xy, the linear interpolant $\mathcal{I}_{\omega_\alpha}[L_{\alpha i}]$ was not subtracted from them because the result, in these cases, would be null modified functions.

In the examples presented herein, it was firstly evaluated the convergence of relative global errors measured by the energy norm (Szabo and Babuška [17]). The exact relative global error ϵ can be calculated as

$$\epsilon = \frac{\|\mathbf{u} - \hat{\mathbf{u}}\|_{\mathcal{E}(\Omega)}}{\|\mathbf{u}\|_{\mathcal{E}(\Omega)}} = \frac{\sqrt{\displaystyle\int_\Omega (\boldsymbol{\sigma} - \hat{\boldsymbol{\sigma}})^{\mathrm{T}} \, \mathbb{C}^{-1} \, (\boldsymbol{\sigma} - \hat{\boldsymbol{\sigma}}) \, \mathrm{d}\Omega}}{\sqrt{\displaystyle\int_\Omega \boldsymbol{\sigma}^{\mathrm{T}} \, \mathbb{C}^{-1} \, \boldsymbol{\sigma} \, \mathrm{d}\Omega}}. \tag{25}$$

The estimated relative error is obtained using the stress recovery procedure presented in Section 3 and replacing the exact stress field by the recovered one in Eq. 25.

Regarding the convergence analysis, five distinct mapped meshes were used in all results that follow. These meshes were obtained using the following number of divisions for the straight lines and arcs of the cylinder, respectively: $4{\times}8$, $8{\times}16$, $16{\times}32$, $32{\times}64$ and $64{\times}128$.

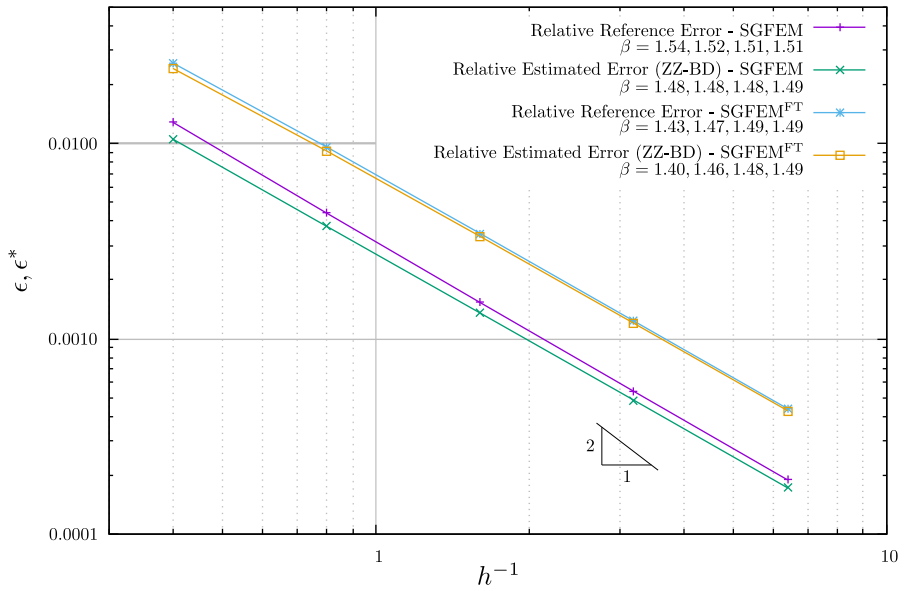

Figure 4. Error convergence in energy norm for SGFEM and SGFEM$^{\mathrm{FT}}$.

The plots presented in Fig. 4 compares the relative exact and estimated global errors (both measured by the energy norm) against the finite element size h^{-1}. Fundamentally, exact errors compare the raw stress field $\hat{\boldsymbol{\sigma}}$ with the exact one $\boldsymbol{\sigma}$ (Eq. 25), while estimated errors compares the raw stress field with the recovered one $\boldsymbol{\sigma}^*$. The proximity of these values can indicate the accuracy of the adopted stress recovery procedure.

All results depicted in Fig. 4 indicates clear agreement between the estimated and exact stresses since the estimated error line plot is very close to the reference one. This feature is even more accentuated for the SGFEM$^{\text{FT}}$ case. Furthermore, in these cases, we can conclude that the error in the recovered stresses will be much smaller than the reference one and this fact also confirms the notable accuracy of the stress recovery procedure for both methods. It can also be observed that the recovered stress results are quite good for both methods, even the error in raw stresses for SGFEM$^{\text{FT}}$ being greater than conventional SGFEM. The plots illustrated in Fig. 4 shows that the convergence rates for the exact and estimated error measures (for both SGFEM and SGFEM$^{\text{FT}}$) is close to the optimal value.

Figure 5 illustrates the raw and recovered stresses $\hat{\sigma}_{xy}$ and σ^*_{xy} distribution for both the SGFEM and SGFEM$^{\text{FT}}$, considering the 4×8 mesh, along with the exact stress distribution.

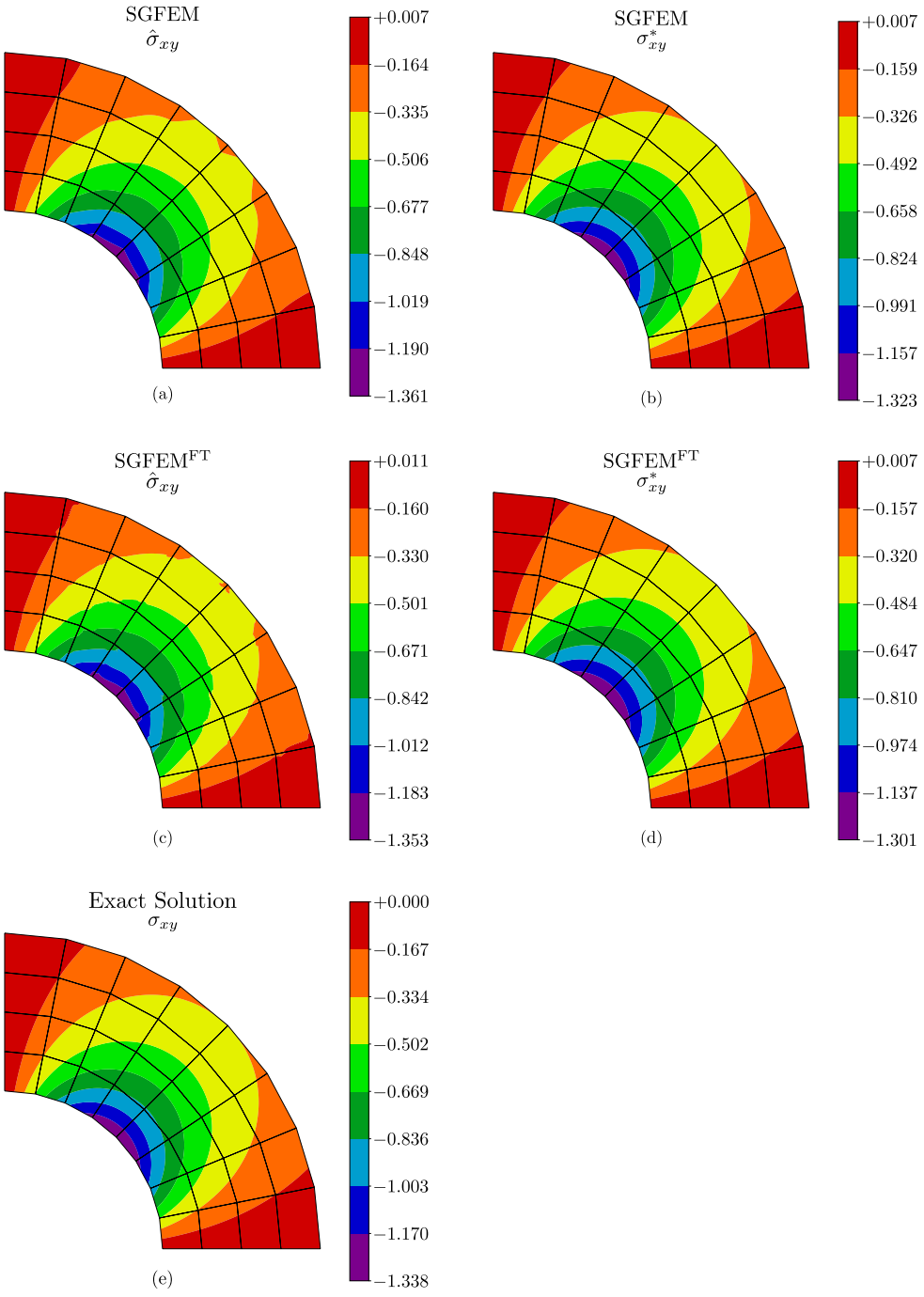

Figure 5. (a) $\hat{\sigma}_{xy}$ and (b) σ^*_{xy} distribution for SGFEM and (c) $\hat{\sigma}_{xy}$ and (d) σ^*_{xy} distribution for SGFEM$^{\text{FT}}$. The exact stress distribution σ_{xy} is presented in (e).

From Fig. 5, we can visually notice a worse initial stress distribution for the SGFEM$^{\text{FT}}$ case, probably caused by the constant regions of φ^* which restricts the polynomial representation of the resulting shape functions. Even with a greater initial global error, the SGFEM$^{\text{FT}}$ can deliver an accurate recovered stress distribution.

Next, Table 1 presents the Scaled Condition Number (SCN) for the matrices $\mathbf{K}$ and $\tilde{\mathbf{A}}$. As already commented in Section 3, $\tilde{\mathbf{A}}$ matrix is equally computed for SGFEM and SGFEM$^{\text{FT}}$, and, by this reason, $\mathfrak{R}(\tilde{\mathbf{A}})$ is the same for both methods.

Table 1. Scaled Condition Number for matrices $\mathbf{K}$ and $\tilde{\mathbf{A}}$ for SGFEM and SGFEM$^{\text{FT}}$.

h^{-1}	N_{dof}	$\mathfrak{R}(\mathbf{K}_{\text{SGFEM}})$	$\mathfrak{R}(\mathbf{K}_{\text{SGFEM}^{\text{FT}}})$	$\mathfrak{R}(\tilde{\mathbf{A}})$
0.4	540	5.49E+19	6.04E+02	1.65E+03
0.8	1836	2.41E+18	5.87E+02	1.72E+03
1.6	6732	3.82E+19	5.72E+02	1.71E+03
3.2	25740	-	1.55E+05	5.64E+02
6.4	100620	-	6.34E+05	5.59E+02

Regarding the results presented in Table 1, it can be noticed the $\mathbf{K}$ conditioning control when SGFEM$^{\text{FT}}$ is applied. Accordingly, one can conclude that the use of different PU along with modified enrichment functions for $\tilde{\mathcal{S}}_{\text{ENR}}$ construction controls the SCN even when smooth polynomial enrichment functions are applied. In general, these functions would induce linear dependencies between the generalized shape functions, a fact that is avoided in the SGFEM$^{\text{FT}}$.

Finally, aiming to compare the stress recovery procedure applied to SGFEM and SGFEM$^{\text{FT}}$, it is then presented the error estimator effectivity index. This measure establishes a comparison between the estimated and the reference global errors and, the closer to the unity is its value, the better the estimator is.

The effectivity index can be calculated as $\theta = \|\mathbf{e}^*\|_{\mathcal{E}(\Omega)}/\|\mathbf{e}\|_{\mathcal{E}(\Omega)}$. Table 2 presents the effectivity index for both SGFEM and SGFEM$^{\text{FT}}$.

Table 2. Effectivity indexes θ for SGFEM and SGFEM$^{\text{FT}}$.

h^{-1}	N_{dof}	θ_{SGFEM}	$\theta_{\text{SGFEM}^{\text{FT}}}$
0.4	540	0.81489	0.93216
0.8	1836	0.85476	0.95304
1.6	6732	0.88383	0.96553
3.2	25740	0.90135	0.97288
6.4	100620	0.91091	0.97697

The results show that the effectivity indexes for the SGFEM$^{\text{FT}}$ are closer to unity than in the SGFEM case. For both methods, the results are suitable, since the effectivity index values tend to unity. The results showed by Table 2 also corroborate to demonstrate the robustness of the ZZ-BD stress recovery procedure since now the raw stresses were provided by SGFEM$^{\text{FT}}$.

4.2 Edge crack panel

The example presented in this section consists of a square panel with an edge crack as that illustrated in Fig. 6. This figure also presents the Dirichlet and Neumann boundary conditions applied to the model. It was assumed Young's modulus $E = 1.0$, Poisson's ratio $\nu = 0.30$ and plane strain conditions.

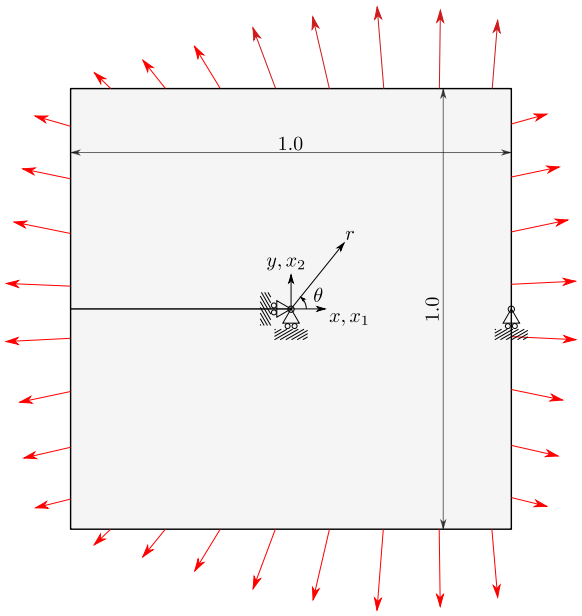

Figure 6. Edge crack panel.

The pressures applied in the panel boundaries (see Fig. 6) refer to the first terms of the asymptotic expansions of the exact solution of pure mode-I stress distribution from Fracture Mechanics, given by the following expressions:

$$\sigma^{\mathrm{I}}_{xx} = \frac{1}{4\sqrt{r}}\left(3\cos\frac{\theta}{2} + \cos\frac{5\theta}{2}\right) \tag{26}$$

$$\sigma^{\mathrm{I}}_{yy} = \frac{1}{4\sqrt{r}}\left(5\cos\frac{\theta}{2} - \cos\frac{5\theta}{2}\right) \tag{27}$$

$$\sigma^{\mathrm{I}}_{xy} = \frac{1}{4\sqrt{r}}\left(-\sin\frac{\theta}{2} + \sin\frac{5\theta}{2}\right) \tag{28}$$

For all analyses performed in this section, it was adopted polynomial enrichment functions $L_{\alpha i} \in \mathscr{P}^2_{\omega_\alpha}$, $\forall\alpha$, and branch functions for the nodes α such as $\mathbf{x}_\alpha \in B_{(C,r)} = \{\mathbf{x} \in \mathbb{R}^2 / \mathrm{dist}(\mathbf{x}, C) \leq r\}$, with $C = (0,0)$ and $r = 0.25$. The branch functions adopted herein correspond to the displacement exact solution around the crack tip (Oden and Duarte [18], Kanninen and Popelar [19]).

$$\mathbf{L}^{x_1}_\alpha = \left\{\sqrt{r}\cos\frac{\theta}{2}\left[\kappa - 1 + 2\sin^2\frac{\theta}{2}\right], \right.$$
$$\left. \sqrt{r}\sin\frac{\theta}{2}\left[\kappa + 1 + 2\cos^2\frac{\theta}{2}\right]\right\} \tag{29}$$

$$\mathbf{L}^{x_2}_\alpha = \left\{\sqrt{r}\sin\frac{\theta}{2}\left[\kappa + 1 - 2\cos^2\frac{\theta}{2}\right], \right.$$
$$\left. -\sqrt{r}\cos\frac{\theta}{2}\left[\kappa - 1 - 2\sin^2\frac{\theta}{2}\right]\right\} \tag{30}$$

with (r, θ) a polar coordinate system attached to the crack tip and κ the Kolosov constant, in which $\kappa = 3 - 4\nu$ for plane strain conditions and $\kappa = (3 - \nu)/(1 + \nu)$ for plane stress conditions.

It is important to mention that when the enrichment functions expressed in Eq. 29 and 30 are used, the recovered stress field is constructed using enrichment functions $L^*_{\alpha i}$ (see Eq. 18) equals to the first terms of the asymptotic expansions of the exact solution of modes I and II stress distributions (these expressions can be found in Lins et al. [7]).

Concerning the convergence analysis, four uniform mapped meshes were used in all results that follow. These meshes were obtained by subdividing the panel sides with the following number of divisions: 8, 16, 32 and 64. As the number of divisions is even, the crack line lies on finite element sides and it was used double nodes to capture its discontinuity.

The plots presented in Fig. 7 exhibits the convergence analysis performed for this example. The plots compare the different error types against the finite element size h^{-1} for SGFEM and SGFEM$^{\text{FT}}$.

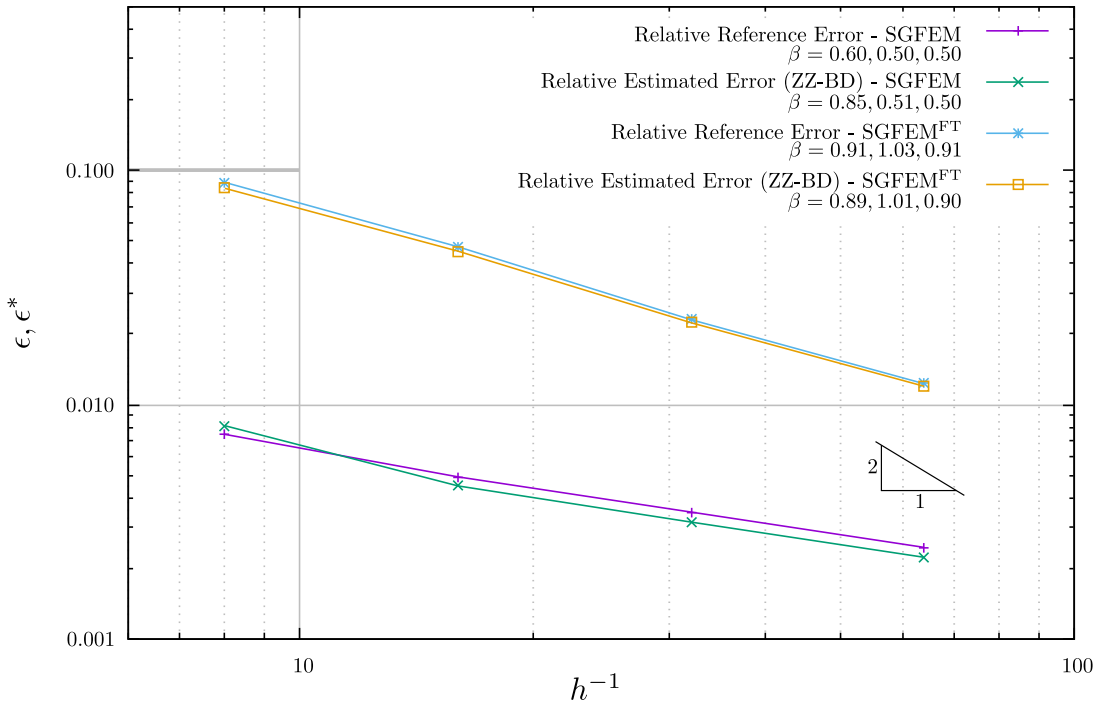

Figure 7. Error convergence in energy norm for (a) SGFEM and (b) SGFEM$^{\text{FT}}$.

As in the previous example, the results presented in Fig. 7 also show good agreement between the exact and estimated error since these line plots are very close to each other. This indicates a desirable performance of the stress recovery procedure for both SGFEM and SGFEM$^{\text{FT}}$ since the recovered stress field can approximate well the exact one. Hence, it can be concluded that the recovered stress field is much more accurate than the raw stress field.

Figure 8, presented next, depicts the von Mises raw and recovered stress distributions for SGFEM and SGFEM$^{\text{FT}}$. Again for the SGFEM$^{\text{FT}}$ case, one can notice a well-behaved recovered stress distribution even with a greater initial global error in raw stress distribution. Figure 8 also shows the exact stress distribution σ_{vm} for the problem.

Regarding the conditioning of SGFEM and SGFEM$^{\text{FT}}$, the Table 3 presents the SCN of matrices $\mathbf{K}$ and $\tilde{\mathbf{A}}$ for both methods.

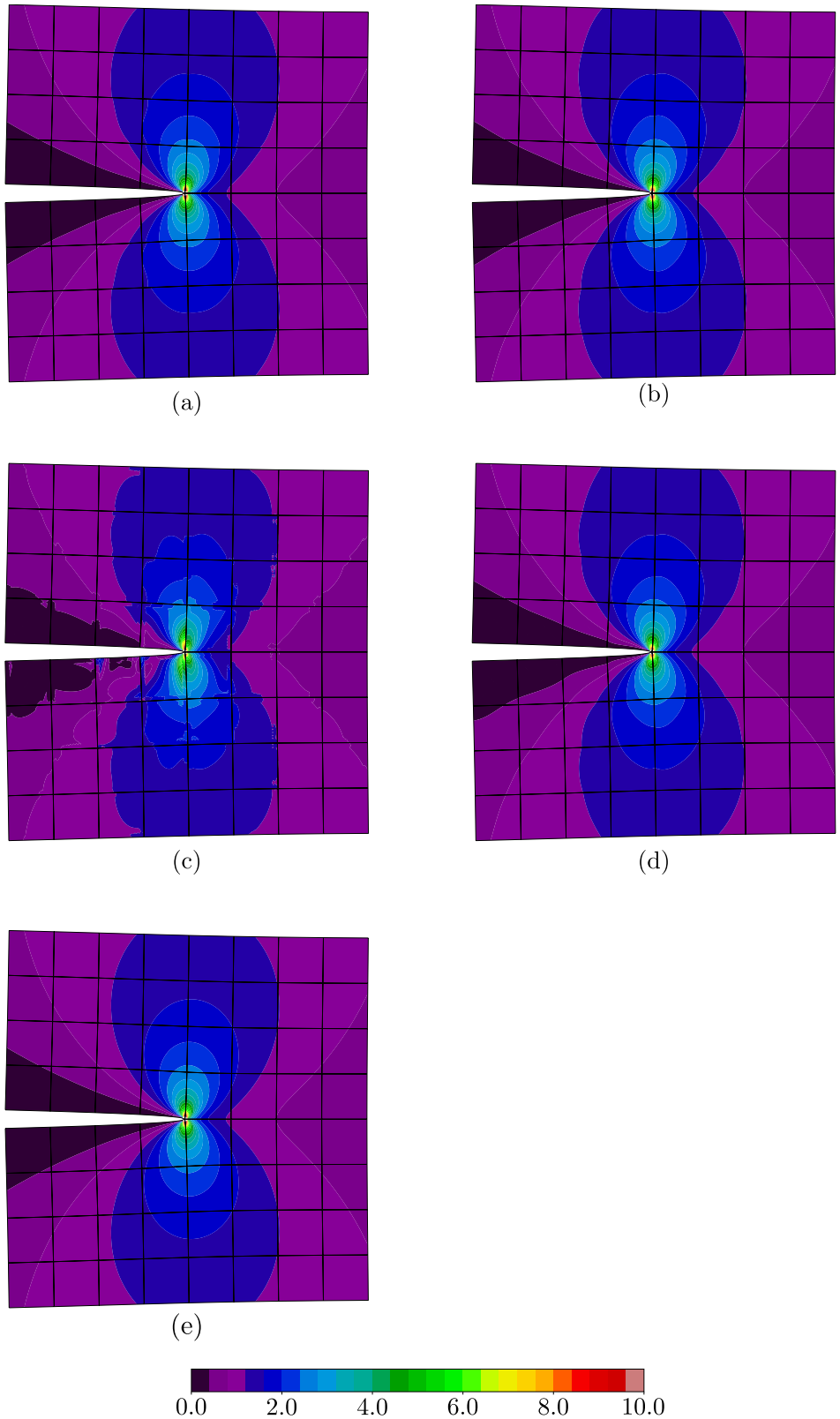

Figure 8. (a) $\hat{\sigma}_{vm}$ and (b) σ^*_{vm} distribution for SGFEM and (c) $\hat{\sigma}_{vm}$ and (d) σ^*_{vm} distribution for SGFEM$^{\text{FT}}$. The exact stress distribution σ_{vm} is presented in (e).

In this example, the SGFEM$^{\text{FT}}$ demonstrates again a good control of the stiffness matrix $\mathbf{K}$ conditioning. For matrix $\tilde{\mathbf{A}}$, the conditioning is kept under control even without modifying the adopted set of enrichment functions and PU.

Table 3. Scaled Condition Number for matrices $\mathbf{K}$ and $\tilde{\mathbf{A}}$ for SGFEM and SGFEM$^{\text{FT}}$

h^{-1}	N_{dof}	$\mathfrak{R}(\mathbf{K}_{\text{SGFEM}})$	$\mathfrak{R}(\mathbf{K}_{\text{SGFEM}^{\text{FT}}})$	$\mathfrak{R}(\tilde{\mathbf{A}})$
8	1080	2.10E+18	3.43E+03	1.49E+05
16	3776	8.32E+18	1.58E+04	1.22E+07
32	14080	2.41E+19	6.99E+04	8.62E+08
64	54336	-	4.16E+05	5.67E+10

Lastly, the Table 4 presents the effectivity index θ for both methods.

Table 4. Effectivity indexes θ for SGFEM and SGFEM$^{\text{FT}}$

h^{-1}	N_{dof}	θ_{SGFEM}	$\theta_{\text{SGFEM}^{\text{FT}}}$
8	1080	1.08875	0.93546
16	3776	0.91472	0.95522
32	14080	0.90652	0.96982
64	54336	0.90680	0.97469

Again, the effectivity index for SGFEM$^{\text{FT}}$ is closer to the unity than in the conventional SGFEM case. Thus, one can conclude that the results of the stress recovery procedure are more evident when applied to that method, probably due to its worse raw stress distribution.

5 Conclusions

Briefly, this work aimed to assess the numerical application of a recently developed stress recovery procedure for the SGFEM$^{\text{FT}}$. The numerical method consists of a GFEM stable version, created to overcome some difficulties presented by the original method as the ill-conditioning of the stiffness matrix that appears mainly due to linear dependencies between its shape functions. This ill-conditioning can lead to numerical solutions polluted by round-off errors, besides compromising the convergence when iterative solvers are used. On the other hand, the stress recovery procedure assessed was firstly addressed by Lins et al. [7] for the conventional SGFEM and consists of a modification in the original Zinkiewicz and Zhu [16] stress recovery procedure, aiming mainly to guarantee a better computational efficiency. In short, it uses a weighted L^2 inner product to generate the system of equations for recovered stresses nodal degrees of freedom, which is formed by a block-diagonal coefficient matrix.

Two examples were presented to evaluate the efficacy of the mentioned stress recovery procedure for both smooth and non-smooth enrichment functions. In these two cases, the recovery procedure proved efficient since the estimated error (computed using the recovered stresses) and the exact error were very close to each other. In other words, this means that the recovered stress field is very close to the exact stress field, returning then a stress distribution which is much better than the original SGFEM$^{\text{FT}}$ raw stresses.

Another advantage of the method verified herein is the control over the stiffness matrix conditioning. In fact, the conventional GFEM may lead to very ill-conditioned stiffness matrices even for smooth enrichment functions and the SGFEM could not guarantee a conditioning control for any adopted set of enrichment functions in 2D and 3D analyses. In the examples presented in this paper, instead of using incomplete polynomials, the second-order complete polynomial functions were used aiming to

reduce the global error and probably this has severely affected the stiffness matrix conditioning in the SGFEM context. For the two examples presented, however, the SCN for the stiffness matrix proved to be controlled when Flat-Top partitions of unity were adopted along with the SGFEM.

Finally, from the examples presented in this paper, it can be seen a good agreement between the use of SGFEM^{FT}, a specific stable version of GFEM, and the ZZ-BD stress recovery procedure. This feature evidences the robustness of ZZ-BD recovery technique. Its application to SGFEM^{FT} can deliver accurate stress distributions with a recovery procedure that spends few computational resources. Further studies with different set of enrichment functions, non-structured meshes and triangular finite elements are being developed for the application of ZZ-BD to SGFEM with Flat-Top Partitions of Unity.

Acknowledgments

The authors would like to acknowledge the support of University of São Paulo (USP) and Aeronautics Institute of Technology (ITA) and the financial support of this research by Coordination for the Improvement of Higher Education Personnel (CAPES) and São Paulo Research Foundation (FAPESP) under process number 2019/00435-3.

References

[1] Duarte, C. A., Babuška, I., & Oden, J. T., 2000. Generalized finite element method for three-dimensional structural mechanics problems. *Computer & Structures*, vol. 77, pp. 215–232.

[2] Strouboulis, T., Copps, K., & Babuška, I., 2001. The Generalized Finite Element Method. *Computer Methods in Applied Mechanics and Engineering*, vol. 190, pp. 4081–4193.

[3] Belytschko, T. & Black, T., 1999. Elastic crack growth in finite elements with minimal remeshing. *International Journal for Numerical Methods in Engineering*, vol. 45, pp. 601–620.

[4] Duarte, C. A., Hamzeh, O. N., Liszka, T. J., & Tworzydlo, W. W., 2001. A generalized finite element method for the simulation of three-dimensional dynamic crack propagation. *Computer Methods in Applied Mechanics and Engineering*, vol. 190, pp. 2227–2262.

[5] Zhang, Q., Banerjee, U., & Babuška, I., 2014. Higher order stable generalized finite element method. *Numerische Mathematik*, vol. 128, pp. 1–29.

[6] Babuška, I. & Banerjee, U., 2012. Stable generalized finite element method (SGFEM). *Computer Methods in Applied Mechanics and Engineering*, vol. 201-204, pp. 91–111.

[7] Lins, R. M., Proença, S. P. B., & Duarte, C. A., 2019. Efficient and accurate stress recovery procedure and a-posteriori error estimator for the Stable Generalized/Extended Finite Element Method. *International Journal for Numerical Methods in Engineering*, vol. -, pp. 1–28.

[8] Gupta, V., Duarte, C. A., Babuška, I., & Banerjee, U., 2013. A stable and optimally convergent generalized fem (sgfem) for linear elastic fracture mechanics. *Computer Methods in Applied Mechanics and Engineering*, vol. 266, pp. 23–39.

[9] Sato, F. M., Piedade, Neto, D., & Proença, S. P. B., 2018. Numerical experiments with the generalized finite element method based on a flat-top partition of unity. *Latin American Journal of Solids and Structures*, vol. 15 (11 Thematic Section), pp. 1–16.

[10] Melenk, J. M. & Babuška, I., 1996. The partition of unity finite element method: Basic theory and applications. *Computer Methods in Applied Mechanics and Engineering*, vol. 139, pp. 289–314.

[11] Prange, C., Loehnert, S., & Wriggers, P., 2012. Error estimation for crack simulations using the XFEM. *International Journal for Numerical Methods in Engineering*, vol. 91, pp. 1459–1474.

[12] Moes, N., Dolbow, J., & Belytschko, T., 1999. A finite element method for crack growth without remeshing. *International Journal for Numerical Methods in Engineering*, vol. 46, pp. 131–150.

[13] Lins, R. M., Ferreira, M. D. C., Proença, S. P. B., & Duarte, C. A., 2015. An a-posteriori error estimator for linear elastic fracture mechanics using the Stable Generalized/Extended Finite Element Method. *Computational Mechanics*, vol. 56, pp. 947–965.

[14] Ramos, C. S., 2019. Partições da Unidade flat-top e trigonométricas no Método dos Elementos Finitos Generalizados. Mestrado, Escola de Engenharia de São Carlos, Universidade de São Paulo, São Carlos.

[15] Schweitzer, M. A., 2013. Variational mass lumping in the Partition of Unity Method. *SIAM Journal on Scientific Computing*, vol. 35(2), pp. A1073–A1097.

[16] Zinkiewicz, O. C. & Zhu, J. Z., 1987. A simple error estimator and adaptive procedure for practical engineering analysis. *International Journal for Numerical Methods in Engineering*, vol. 24, pp. 337–357.

[17] Szabo, B. & Babuška, I., 1991. *Finite Element Analysis*. John Wiley and Sons, New York.

[18] Oden, J. T. & Duarte, C. A., 1996. Solution of singular problems using h-p clouds. In *MAFELAP 96*.

[19] Kanninen, M. F. & Popelar, C. H., 1985. *Advanced Fracture Mechanics*. Oxford University Press, New York.